Research Article Vol. 4, No. 3 / 15 March 2021 / OSA Continuum 940
OSA CONTINUUM

Picosecond thin-disk laser platform PERLA for multi-beam micromachining

MARTIN SMRŽ,[1,*] JIŘÍ MUŽÍK,[1,2] DENISA ŠTĚPÁNKOVÁ,[1,2] HANA TURČIČOVÁ,[1] ONDŘEJ NOVÁK,[1] MICHAL CHYLA,[1] PETR HAUSCHWITZ,[1,2] JAN BRAJER,[1] JAN KUBÁT,[3] FILIP TODOROV,[4] AND TOMÁŠ MOCEK[1]

[1] *HiLASE Centre, Institute of Physics of the CAS, Za Radnicí 828, 252 41 Dolní Břežany, Czech Republic*
[2] *Czech Technical University in Prague, Faculty of Nuclear Sciences and Physical Engineering, Dept. of Physical Electronics, Trojanova 13, 120 01 Prague 2, Czech Republic*
[3] *Crytur s.r.o., Na Lukách 2283, 511 01 Turnov, Czech Republic*
[4] *Institute of Photonics and Electronics of the CAS, Chaberská 1014/57, 182 51 Prague 8, Czech Republic*
[*] *martin.smrz@hilase.cz*

Abstract: Multi-beam micro- and nano-machining of material surfaces has been getting more important because of its great potential to increase production speed of large size laser induced periodic surface structures (LIPSS). Fast and cheap production of engineered surfaces structures can bring unique properties of surfaces like tailored wettability, friction, antibacterial properties, etc., to mass-production with consequence in, for example, energy and costs savings. However, tailoring of long-term stable interference patterns from ultrashort laser pulses requires an extremely stable laser system with nearly diffraction-limited output beams. HiLASE Centre developed such a thin-disk-based Yb:YAG sub-picosecond laser platform, PERLA, providing average output power up to 0.5 kW with 2nd and 4th harmonic generation extensions and demonstrated its potential for direct laser interference patterning (DLIP). In this paper, we focus on details of the thin-disk PERLA laser.

1. Introduction

Adoption of picosecond lasers for micromachining has recently been accelerated thanks to increase of available average power. These lasers are ideal candidates for surface micro-structuring, highly precise cutting, drilling, etc. Surface structures on processed materials have frequently periodic nature, which can lead to an engineered modification of surface properties of large size components like wettability, friction, antibacterial properties, etc. The surface functional performance originates in hierarchical structures composed of micro and nanoscale features assembled into complex structures. Such surface modifications are called Laser Induced Periodic Surface Structures (LIPSS) [1]. Variety of techniques for replicating naturally occurring microstructures, including chemical vapor deposition, chemical etching, sol-gel, plasma treatments, lithography, or electrodeposition exist. Among all the techniques, laser surface texturing provides a flexible, fast, and environmentally friendly approach for the high precision fabrication of desired micro and nano-geometries [2,3].

2. Multi-beam micromachining

There are basically two ways leading towards large size laser-induced micro- and nano-structures. First, surface treatment at moderate pulse energy and high repetition rate of a pulsed laser system, ideally several MHz, in combination with very fast galvo scanners. However, this may not satisfy high industrial demands for the treatment of large areas in short time. Additionally, recent increase in average power of ultrashort laser system does not bring the desired increase in

#418293 https://doi.org/10.1364/OSAC.418293
Journal © 2021 Received 23 Dec 2020; revised 11 Feb 2021; accepted 12 Feb 2021; published 3 Mar 2021

efficiency of micro- and nano-machining, because only small portion of the available laser power is used for machining to maintain high quality as well as to avoid melting and thermal effects on work pieces. In addition, the fast process is demanding for both laser construction and process control with synchronization [4,5].

Alternatively, multi-beam processing techniques can be employed [6,7,8]. Multi-beam processing techniques are suitable for high energy picosecond lasers with highly spatially coherent diffraction-limited laser beams with high positioning and high pulse energy stability. A way towards the multi-beam interference patterns leads through integration of optical elements splitting the beam into clones of themselves into an optical setup, and creation of conditions for their defined overlapping. This approach is especially interesting for high-energy high-beam-quality thin-disk regenerative amplifiers with multi-kHz repetition rate, like the thin disk laser platform PERLA developed at the HiLASE Centre in Czechia [9].

3. Yb:YAG thin-disk lasers

Thin disk laser geometry was developed in early 90's like a scalable platform for diode-pumped industrial lasers [10]. Since its invention, thin-disk lasers have been undergoing hundreds of improvements including power and energy scaling. Nowadays, thin-disk lasers generate near-infrared radiation from continuous-waves (CW) down to few-cycle femtosecond pulses in temporal domain, exceed average power of 4 kW in diffraction limited beams, and 12 kW in multi-mode regime [11–13]. Pulse energy from a single Yb:YAG thin disk regenerative amplifier can approach single pulse energy of 600 mJ [14], and picosecond multipass thin-disk-based booster amplifiers reached energy level of 800 mJ with repetition rate up to 1 kHz recently [15].

Thin disk lasers have several advantages over rod-type solid state lasers facing serious problems with thermal lensing and material expansion due to thermal gradients generated in a volume gain media. In pulsed regime, pulse propagation in the bulk induces nonlinear response resulting in, besides other effects, self-focusing of laser beams inside the rod. Both phenomena can consequence in significant changes in laser behavior and damage on optical components of the laser itself. The thin-disk gain medium acting a role of an extremely thin active mirror prevents that behavior, namely because of large mode size and much higher doping concentration in comparison with rods, which leads to reduction of material beam path and accumulated B-integral. The gain medium with an antireflective (AR) coating on a front side, and a highly reflective (HR) one on a back side, serves as a mirror for both pump and signal beams. Thin disks are usually attached to a water-cooled heatsink extracting waste heat efficiently in an axial direction of the thin-disk through the HR coated surface and supporting the disk mechanically.

Because of small thickness and low single-pass absorption of thin disk gain media, optical systems consisting of a parabolic mirror and several reflecting prisms realizing multiple passes of a pump beam are used [16,17]. We use a configuration with two roof mirrors and 24 or 36 pump beam passes (Fig. 1), however, configurations suitable for 48 and more pump beam roundtrips were proposed [18]. Total pump beam absorption exceeding 90% can be reached this way. Achievable size of a pumped area and pump power density on a thin-disk depends on brightness of a pump source and focal distance of an image-relaying optics, which is usually 50–150 mm. Pump mode size D on a thin disk for our setups with fiber coupled diodes and fiber core diameter d can be simplified like magnification of the parabolic mirror and a fiber collimation lens where f_{par} and f_{col} are focal distances of the parabolic mirror and the collimator, respectively

$$\frac{D}{d} = \frac{f_{par}}{f_{col}}$$

Although many materials have been demonstrated in thin disk geometry already, by far the most common one is Yb-doped YAG ($Y_3Al_5O_{12}$) emitting at wavelength of 1030 nm. Thanks to Yb^{3+} ions with quasi-three-level structure reaches this gain medium very high efficiency.

OSA CONTINUUM

Isotropic YAG crystals provide chemically and mechanically very stable matrix for Yb ions. They can be grown in large pieces and cheaply polished to thickness bellow 100 µm while keeping high overall flatness and small roughness of the surface (R_a parameter). For example, Czech crystal manufacturer Crytur can grow boules up to 150 mm in diameter [19,20], and polish surface of thin-disks to $R_a \leq 0.3$ nm. Yb:YAG can be pumped [21] by cheap and widely available high brightness laser diodes in a broad absorption peak close to wavelength of 940 nm, or by narrow-band volume Bragg grating (VBG) stabilized diodes emitting at 969 nm. Pumping at 969 nm is so called zero-phonon line pumping exciting electrons directly to upper laser level, which reduces quantum defect from 8.7% to 5.9%, and, as a consequence, amount of waste heat generated in the laser crystal is 32% decreased [22]. Besides the quantum defect, we showed in the past that nonlinear phonon relaxation effects occur during the conventional pumping at 940 nm, which generate additional heat causing nonlinear increase of thin-disk temperature, unlike the zero phonon line pumping where this effect absents [23,24].

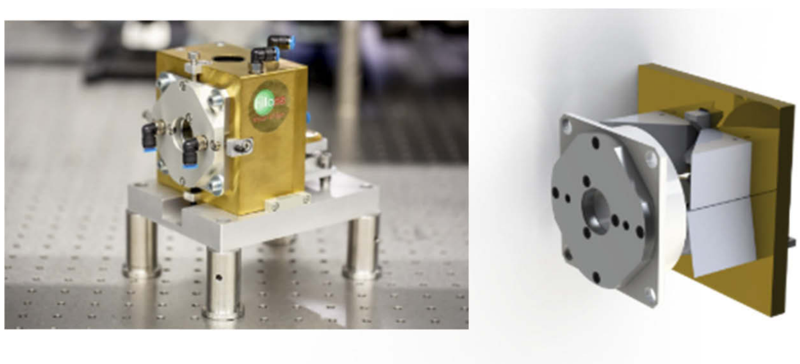

Fig. 1. Photo (left) and model of mirrors (right) of the in-house developed laser head for efficient pumping of thin-disk modules with inner part consisting of a parabolic mirror and two roof mirror retro-reflectors for realization of 36 pump beam passes through a gain medium.

Thick heatsink of the thin disk with high thermal conductivity provides efficient and homogeneous heat extraction from the disk, and serves as its mechanical support preventing the thin-disk from bending. Therefore the frequently used material for supporting the disks has become lately synthetic diamond. Optimal working condition is keeping the disk as close to cooling temperature as possible but the real conditions are often different. Matching of thermal expansion coefficients of Yb:YAG and diamond is not optimal, and edges of pumped area on the disk create a step-like transition in disk temperature. High mechanical strain or stress generating optical path difference (OPD) as a consequence of generated thermal gradients therefore exists. Spatially dependent OPD generates wavefront deformation in laser beams passing the gain medium. The OPD can be decomposed into spherical part leading to defocus, and aspherical part causing higher order aberrations. The spherical one is easier to compensate by resonator optics but the aspherical deformation permanently deteriorates beam quality [23,25,26].

Thin disk deformation can be minimized through optimization of the disk module construction, however, the bonding technology between the active medium and the heatsink remains a bottleneck of the thin disk technology. The joint of both materials must transfer efficiently waste heat and absorb all mechanical forces coming from mismatch of material thermal expansions and from temperature gradients. Epoxies are working very well mechanically but they have extremely low thermal conductivity. Since demands for surface quality preparation in case of epoxy bonded disks are not so extreme, they are widely used and can serve well up to kilowatts of average output power of laser systems. We demonstrated also epoxy-free bonding which could

OSA CONTINUUM

bring in the future next improvements of thin disk performance. The technology reduces OPD caused the by thin disk bending and reduces also thin disk temperature. On the other hand, epoxy-free technology is very demanding for low roughness (R_a) of the disk surface needed for the bonding. We successfully demonstrated atomic diffusion bonding (ADB) of Yb:YAG disks to metallic substrates by recrystallization of a thin gold layer deposited on both attached surfaces [27]. This was just first step and next development of this technology continues. Although the demonstrated results of our PERLA 100 and PERLA 500 were reached with epoxy-bonded disks, we expect adoption of the directly bonded disks to PERLA 500 technology for multibeam material processing in the future. Besides more effective cooling, the negligible OPD of the ADB disks under high thermal load is the key important for excellent beam quality at high average power.

4. PERLA 100 and PERLA 500 laser platform

The PERLA thin-disk laser platform developed at HiLASE adopts the well-known CPA (Chirped Pulse Amplification) technique [28] preventing laser induced damage on ultrashort laser pulse amplifiers. We have developed two modifications of the platform, PERLA 100 for systems working up to 100 W of average power, and PERLA 500 for power up to 500 W. Especially the PERLA 100 platform is currently operated and being constructed at HiLASE in several pieces, each optimized for slightly different pulse energy in a range from 0.5 mJ to 20 mJ, and repetition rates from 200 kHz to 2.5 kHz, respectively.

PERLA 100 (Fig. 2) is designed as a fiber-based front-end followed by a thin disk based high power regenerative amplifier. PERLA 500 is currently an extension adding a second stage high-power regenerative amplifier. Finally, the pulses are compressed by a chirped volume Bragg grating, or a transmission dielectric grating-based pulse compressor. In all cases, 8-picosecond-long chirped seed pulses with nanojoule pulse energy and repetition rate of 40 MHz are produced by the GoPico Yb-doped fiber oscillator. Seed pulse bandwidth is ≈ 20-nm (FWHM), central wavelength 1028 nm. The oscillator is based on all normal dispersion mode-locking technique (ANDi) [29] and was fully developed at HiLASE Centre. The oscillator was designed in regards to high stability of the output pulse train and immunity to stochastic mode instabilities [30,31]. The pulses from the oscillator are further stretched by a chirped fiber Bragg grating stretcher (CFBG). Dispersion of the stretcher is chosen with regards to the target pulse energy. The optimal stretched pulse duration for pulse enegy up to 20 mJ is approximately 500 ps. Stretcher chirp rate is ≈ 205 ps/nm in this case. The stretcher contains baseplate able to generate thermal gradient along the grating and so slightly tune the dispersion, which is useful for example in a pair with a chirped volume Bragg grating pulse compressor with fixed value of dispersion. Pulse bandwidth is clipped in the stretcher to 3.5 nm (full spectral width) because of technological limits on product dispersion and bandwidth of CFBGs. The pulse stretcher is followed by a pair of Yb-doped single-mode fiber preamplifiers with an acousto-optic pulse picker inserted between the amplifiers. The first pre-amplifier amplifies pulses entering the fiber-coupled pulse picker with high insertion loss to prevent significant drop of signal-to-noise ration after passing it. The fiber-coupled pulse picker reduces pulse repetition rate to 1 MHz, which was selected like a compromise between sufficient boosting of pulse energy in thesecond fiber amplifier, and suppression of amplified spontaneous emission and scattering in the pre-amplifiers. Both pre-amplifiers are pumped by single-mode fiber-coupled laser diodes emitting at central wavelength of 976 nm. Finally, the pulses are sent to the PERLA 100 thin disk amplifier.

The PERLA 100 main amplifier is designed as a regenerative amplifier system with a standing-wave cavity. It contains a single diamond-bonded Yb:YAG thin disk with doping concentration of 7.2% and thickness of 220 µm. The thin-disk is pumped continuously at wavelength of 969 nm by fiber-coupled VBG stabilized diodes. Diameter of the pumped area is 2.8 mm. Pulse locking in the amplifier cavity is based on polarization switching by application of quarter wave voltage

OSA CONTINUUM

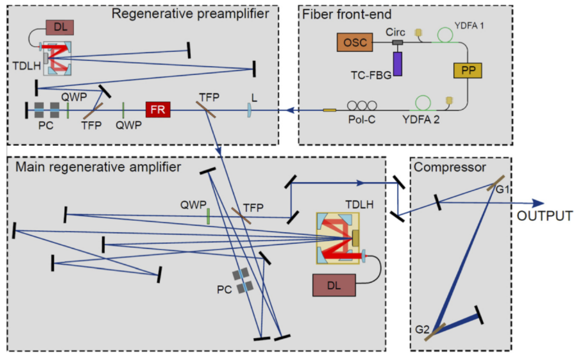

Fig. 2. Optical scheme of PERLA C laser system consisting of a fiber front-end, PERLA 100 regenerative amplifier with a standing wave cavity, PERLA 500 high power regenerative amplifier with a ring cavity, and a transmission dielectric diffraction grating-based pulse compressor; TDLH – thin-disk laser head, PC – Pockels cell, DL – pump diode laser, FR – Faraday rotator, TFP – thin film polarizer, L – lens, QWP – quarter wave plate, OSC – oscillator, Circ – circulator, YDFA – Yb-doped fiber amplifier, TC-FBG – temperature-controlled fiber Bragg grating, PP – pulse picker, Pol-C – polarization controller, G – diffraction grating.

to a pair of BBO crystals with $8 \times 8\,\mathrm{mm}^2$ aperture in a Pockels cell. Pair of crystals is used to reduce control voltage, which can exceed 4 kV even in this configuration. Cavity is designed for efficient amplification of TEM_{00} spatial mode only, and number of roundtrips is typically >50 due to low single-pass gain of thin-disks. Real number of roundtrips is optimized for full extraction of stored pulse energy at given repetition rate. Timing of the amplifier also takes into account prevention of bifurcations [32], which can occur at some pulse repetition rates. Repetition rate is controlled by triggering of the Pockels cell, and is derived from the oscillator clock like its integer quotient. Proper design of a laser cavity together with diamond bonded thin-disks are important for high beam quality at high average power. Simple cavity scheme currently used for a regenerative amplifier working at 100 kHz is shown in Fig. 2. We managed to extract pulse energy > 1 mJ at repetition rate of 100 kHz from this cavity with opt.-opt. efficiency >35% (Fig. 3) [33]. Slope efficiency is 41.5%. PERLA 100 platform developed at HiLASE is currently at technical readiness level (TRL) 6–7 (Fig. 4) with beam quality $M^2 = 1.1$ and long term power fluctuation below 0.2% (r.m.s. value).

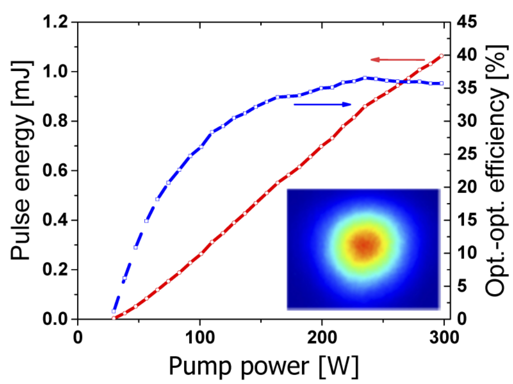

Fig. 3. Output pulse energy (red line), opt. – opt. efficiency (blue line), and near field beam profile of PERLA 100 regenerative amplifier operating at 100 kHz.

OSA CONTINUUM

Fig. 4. PERLA 100 thin-disk regenerative amplifier (top) with a preamplifier module (bottom, left) and GoPico ANDi fiber oscillator (bottom, right) [43].

PERLA 500 is a second amplifier of the above described laser system (Fig. 2). PERLA 100 serves as a first amplifier of the system, although not the full power is used for seeding. Optimal seed pulse energy for extraction of >5 mJ at 100 kHz is 0.2 mJ, which is about 20% of the PERLA 100 capability. A new front-end with a rod-type preamplifier for PERLA 500 replacing the PERLA 100 is therefore under development. PERLA 500 is designed like a regenerative amplifier with a ring cavity. The disk is inserted into a ring cavity with two V-passes through the thin-disk per one cavity roundtrip. Footprint area of this amplifier is only 100×60 cm^2. Ring cavity has several advantages over a standing wave cavity. First, it does not need large size Faraday rotators for separation of input and output beams. Second, for given mode size, a ring cavity is shorter than a standing wave cavity with the same mode size. Third, it does not need any isolator between the pre-amplifier and the main amplifier because of spatially-separated input and output. Scaling of the amplifier to higher pulse energy and towards 0.5 kW requires pump mode size of 5.2 mm on the thin-disk. As a pump source serves a VBG-stabilized fiber-coupled diode module delivering up to 1.5 kW in continuous-wave at wavelength of 969 nm. Polarization switching of the amplifier is realized by a Pockels cell with a pair of BBO crystals with $10 \times 10\,\mathrm{mm}^2$ aperture installed in an in-house developed water-cooled holders enabling to apply switching pulses up to 10 kV. The cavity can be operated at 100 kHz or 50 kHz. For comparison, we operated the cavity in CW with maximum output power of 565 W with 1.21 kW of pump power, optical-to-optical efficiency of 47%, and slope efficiency of 55%. In seeded operation with the input pulse energy of 0.2 mJ, output pulses with 4.5 mJ of pulse energy at 100 kHz repetition rate, extraction efficiency of 43%, and slope 39.6% were demonstrated. At the repetition rate of 50 kHz, 9 mJ pulses were generated (450 W) with 1130 W of pump power, optical-to-optical efficiency of almost 40%, and 44.6% slope (Fig. 5(a)).

Bandwidth of output pulses from the PERLA 100 and PERLA 500 was 1.3 nm and 1.4 nm (FWHM), respectively. Bandwidth of 1.4 nm theoretically allows pulse compression down to 650 fs. Figure 5(b) shows all the measured spectra. Unlike expected gain narrowing in the regenerative amplifiers, we observed spectral reshaping and small broadening of the bandwidth from 1.2 nm after passing the front-end. This is given by shifted emission peak of the Yb-doped fiber preamplifiers, and the Yb:YAG main amplifiers. In the 50-kHz regime, a several-hour-long stable operation was demonstrated with an average output power of 330 W (6.4 mJ) in fundamental transverse mode, as shown in Fig. 5(a) (inset). The laser was operated for 10 hours at 330 W with a power fluctuation as low as 1.2% (r.m.s.). Technical readiness level of this amplifier is at level 4–5. Increase of the TRL level and upgrade towards 1 kW are under development.

OSA CONTINUUM

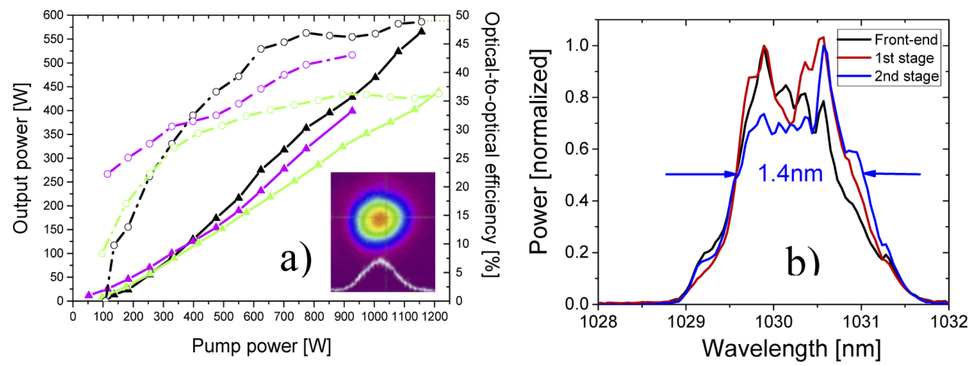

Fig. 5. (a) Output power (solid), opt.-opt.efficiency (dashed), and near-field beam profile of the PERLA 500 in CW operation (black), pulsed operation at 50 kHz (violet), and 100 kHz (green) repetition rate [9]; (b) comparison of output spectra of the fiber front-end, PERLA 100 regenerative amplifier, and PERLA 500 regenerative amplifier.

5. Specifics of high power pulse compression

PERLA platform like majority of high-energy ultrashort pulse generating lasers is adopting CPA technology. Pulses stretched in the front-end to sub-nanosecond temporal range need to be compressed back to sub-picosecond transform limit. Two different approaches to pulse compression were compared in the PERLA platform, chirped volume Bragg grating (CVBG) and a pair of transmission dielectric gratings. It turned out the CVBG is solution suitable for low power, low pulse energy systems but in lasers like PERLA 500 leads to significant reduction of laser beam quality.

A CVBG is a reflecting grating holographically recorded inside a volume of photo-thermo-refractive (PTR) glass [34] with a gradually variable period of refractive index modulation in the direction of beam propagation. The most significant assets of a CVBG are its small size (typical volume on the order of several cm^3), resistivity to shocks and vibrations [35], easy adjustment, and independence on polarization. A CVBG can also provide a large amount of dispersion. In the PERLA system we used CVBGs with dispersion value of 205 ps/nm. The CVBG was designed for bandwidth of 3.3 nm (full width at $1/e^2$ of max.) and central wavelength of 1030.3 nm. Input and output beam were separated by a thin film polarizer and a quarter wave plate rotating linear polarization direction by 90° in double pass configuration (Fig. 6(a)). Monitored parameters during system optimization were, besides pulse duration and output spectrum, also beam quality, net-efficiency, and surface temperature. The limiting factor in case of the 0.5 kW laser system turned out to be residual heat absorption in the PTR glass and way of its mechanical fixation. For loosely mounted grating we observed similar behavior of the grating in x and y direction unlike spring fixing mechanism case used for comparison. We demonstrated usability of chirped volume Bragg gratings for beams up to approximately of 100 W of average power. For average power up to 100 W ranged the beam quality described by M^2 parameter from 1.75 to 2.0. The M^2 parameter increased to 3.0 at 200 W and to 3.4 at 269 W, when we stopped our measurement because of risk of damage (Fig. 6(b)) [36]. At the same time we measured increase of pulse duration from 1.4 ps at low power to 2.4 ps (FWHM) at full power. Pulse duration slightly reduced to 1.9 ps after fine stretcher dispersion tuning, however, high pedestal was obvious from the intensity autocorrelation trace (Fig. 7(a)). Diffraction efficiency dropped from 84% to 80% with rising average power. Measured data were later supported by a numerical calculation explaining partially the grating behavior and advent of the high pedestal with rising average power [37].

Since the CVBG-based pulse compression showed up to be applicable to lasers well below 100 W of average power, and the multi-beam processing as the target application demands the

OSA CONTINUUM

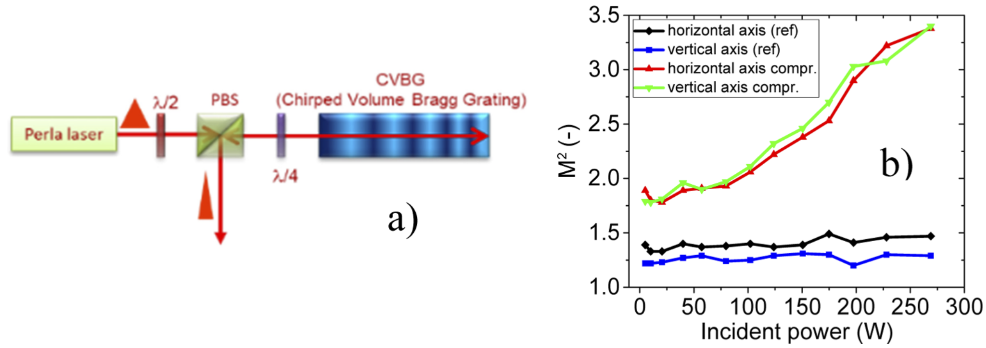

Fig. 6. (a) Optical scheme of the coupling of a stretched laser beam to the CVBG pulse compressor; (b) degradation of M^2 parameter of compressed laser beam with rising average output power. For comparison, data obtained by a reference flat mirror instead of the CVBG is shown [36].

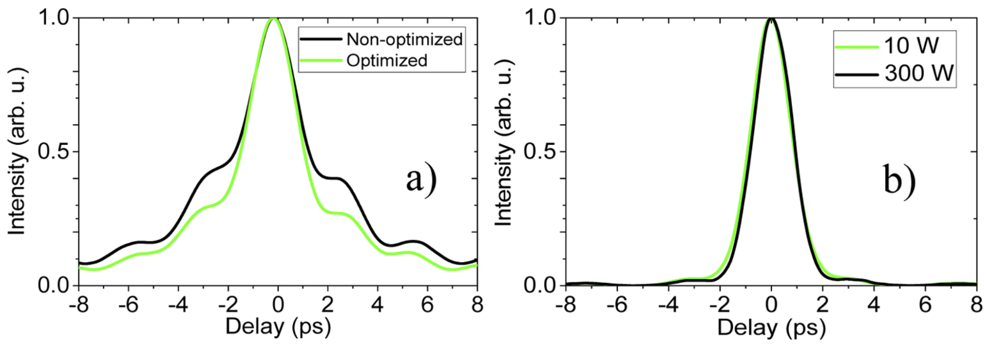

Fig. 7. (a) Intensity autocorrelation traces of pulses compressed by the CVBG compressor in 269 W laser beams, compared for optimized (green) and non-optimized (black) dispersion of the whole laser chain [36]; (b) Intensity autocorrelation traces of pulses compressed by the Treacy-type compressor, comparison for 300 W and 10 W laser beams.

parameter as low as possible, we designed a Treacy-type compressor [38] based on a pair of transmission dielectric diffraction gratings with a roof mirror retroreflector. The gratings made by Jenoptik had 1840 lines/mm. The compressor was designed for Littrow angle of 71.5°. For the required dispersion of 205 ps/nm was the perpendicular gratings distance 91 cm. We tested the same pulse compressor for both PERLA 100 and PERLA 500 platforms. The best achieved pulse duration was 1.0 ps (FWHM) from PERLA 500 regardless output average power (Fig. 7(b)), and 0.9 ps from the PERLA 100. Side lobes caused probably by uncompensated higher order dispersion observed in intensity autocorrelation of the CVBG compressor were almost suppressed with the dielectric-gratings-based compressor. Net efficiency of the compressor reached 99%, and beam quality at 249 W given by M^2 approximately 1.3 and 1.4 in horizontal and vertical axes, respectively. PERLA 100 platform provides as good beam as 1.1 in both axes with this compressor, which is excellent for DLIPs and other techniques of multi-beam micromachining.

6. Harmonic generation for the PERLA platform

The usability of PERLA platforms is extended by the generation of harmonic frequencies. Besides the second harmonic of 515 nm also the third (343 nm), fourth (257.5 nm) and fifth (206 nm) are generated in sum frequency processes, for a block scheme see Fig. 8 [39,40].

OSA CONTINUUM

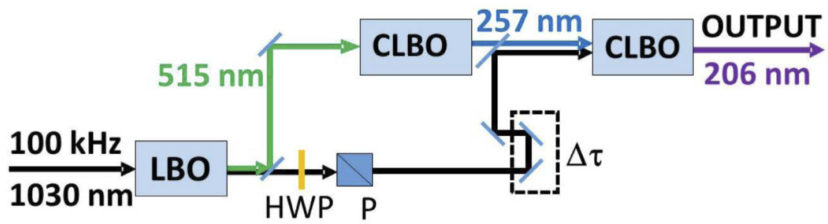

Fig. 8. Schematic of the harmonics generation system at PERLA C. The CLBO crystals are kept at 150°C in nitrogen atmosphere.

Picosecond pulses of the UV and deep UV (below 300 nm) radiation are used for specific processing of materials, such as very precise microstructures with sharp edges and high aspect ratios [41] and stimulation of surface phase transitions [42]. The following figures present the dependences of the second harmonic on the fundamental beam power of PERLA 500 (Fig. 9(a)), and the fourth harmonic on the second harmonic (Fig. 9(b)). The best values attained for picosecond pulses were 76 W in second harmonic and 11 W in fourth harmonic from 136 W in fundamental. Long-term power fluctuation (r.m.s. value) at 41 W of the 515 nm beam, and 6.5 W of the 257.5 nm beam, measured over period of 1 hour was 0.8% and 1.2% at the second and fourth harmonic frequency, respectively. The harmonics system enables also the generation of the third harmonic (maximum 38 W, sum frequency generation 2 ω + 1 ω) and fifth harmonic (maximum 1.5 W, SFG 4 ω + 1 ω). The harmonics system is equipped with a user box where the samples, if necessary water cooled, can be treated with any of the harmonics mentioned above. Beam quality of second harmonic frequency generation and its power stability is given primarily by properties of fundamental beams. The best beam quality was reached at PERLA 100 platform where the beam quality approached $M^2 = 1.2$.

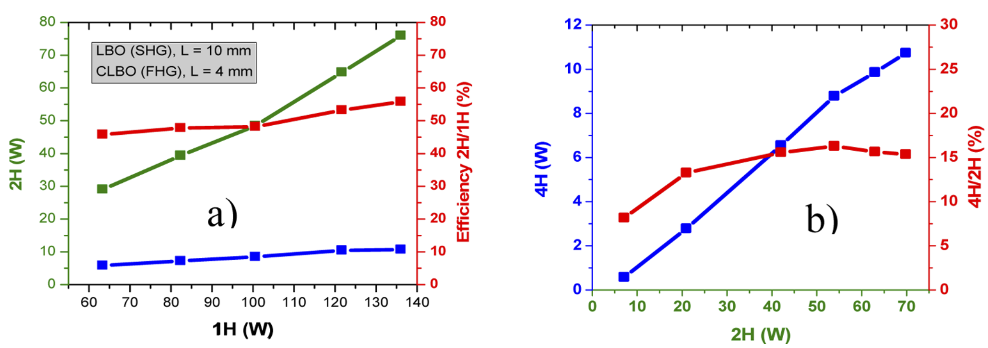

Fig. 9. (a) Output power (green) and conversion effciency (red) of second harmonic frequency (515 nm) and output power of fourth harmonic frequency (blue) pumped by PERLA 500 laser; (b) Output power of fourth harmonic frequency and conversion efficiency (red) for conversion from second harmonic frequency (515 nm) in CLBO crystal.

7. Applications of the PERLA platform for industrial micro-processing

For synchronization with experimental setup, electro-optic pulse picker based on a pair of BBO crystals is used. The setup is equivalent to Pockels cells used for the regenerative amplifier switching. Application potential of PERLA platform was demonstrated on single- and multi-beam material processing at fundamental, second, and third harmonic frequency. For example, integration of thin-disk PERLA lasers with diffractive optical elements allows for fast large-size

OSA CONTINUUM

patterning by direct laser interference patterning (DLIP) with kHz pulse trains. This large size multi-beam interference was demonstrated on AISI 316L steel, invar, or tungsten (Fig. 10) at fundamental wavelength [7,8]. Pulses with energy up to 3 mJ at repetition rate of 1 kHz (wavelength 1030 nm) created 25 µm hole raster, fluence up to 0.17 J/cm^2 and hole diameter up to 20 µm in case of 4-beams interference. The treated area in a single step had diameter of ≈ 1.5 mm. All beams were identically linearly polarized, perpendicularly to the fine structure in the spots (Fig. 10(c)). 2-beams interference (Fig. 10(e)–(g)) with fluence up to 2.44 J/cm^2 (3 mJ) formed lines with periodicity of 2.67 µm.

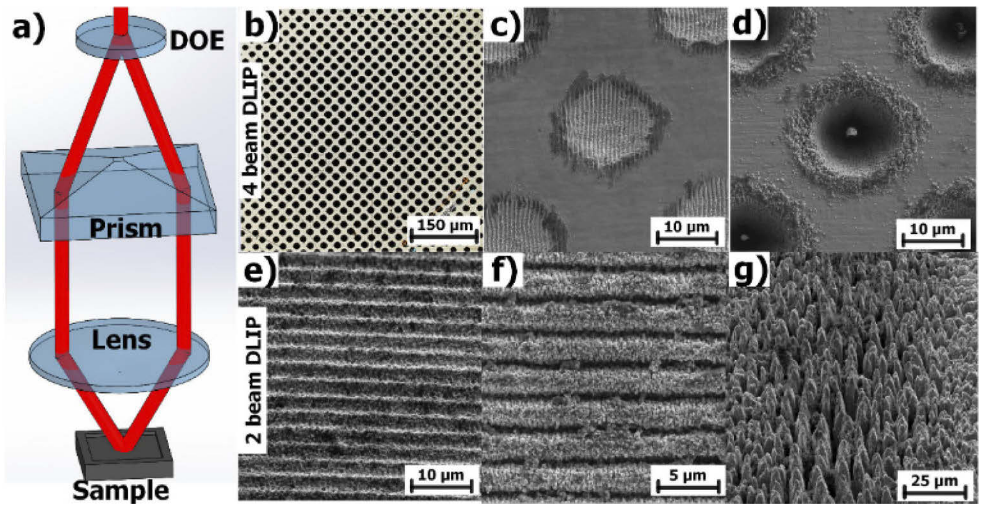

Fig. 10. Example of 2 and 4 beam interference processing on ASISI 316L steel. (a) schematics of interference station; (b) overview of 4-beam interference pattern; (c) LIPSS structure formed after first 5 pulses during 4-beam DLIP (0.17 J/cm^2); (d) drilling with 4-beam DLIP; (e-f) functional structures made by 2-beam DLIP with different pulse energy.

Single beam cutting and drilling of thin Ce:YAG crystals was demonstrated on second harmonic frequency of the picosecond PERLA laser with pulse energy of 30 µJ and focal spot size of 15 µm. Application of the target products demanded realization of sharp edges, even for extraordinary shapes of cuts realized on 0.2 and 0.5 mm thick crystalline slabs. Crucial in this process is to prevent micro-cracks and other damages at material edges since such damages significantly reduce efficiency of the final devices assembled from the Ce:YAG components. Limiting for the cut width is material thickness – the cut cannot be narrower than one fifth of the material thickness to reach the sharp edge. Figure 11 shows excellent results of preliminary tests by the thin disk laser PERLA at repetition rate of 1 kHz, however, final cutting procedure is being optimized at repetition rate of PERLA laser ≈ 200 kHz, which reduces processing time.

OSA CONTINUUM

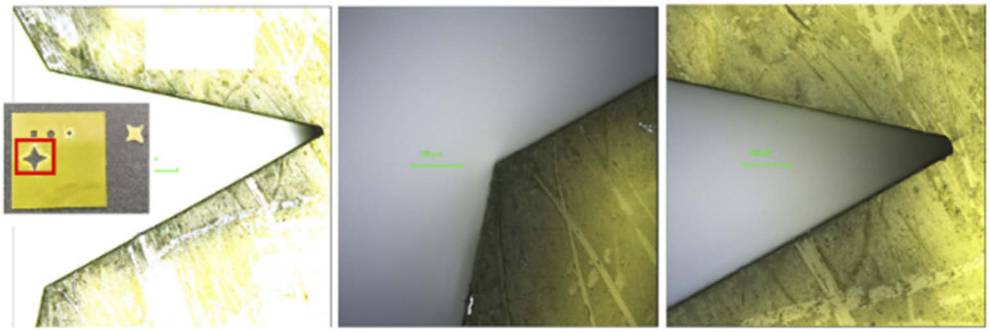

Fig. 11. Cutting of 500 µm thick slab of Ce:YAG (Crytur) by the second harmonic frequency of the picosecond laser PERLA (pulse energy 30 µJ). The figures show details of steep edges which are processed without any micro-cracks, even in corners.

8. Summary

Thin disk lasers undergone long way since their invention in 1991. Nowadays they deliver kilowatt output power from continuous waves to high energy ultrashort pulses, especially in combination with Yb:YAG gain media. HiLASE Centre developed kW-class PERLA 100 and PERLA 500 picosecond thin disk laser platforms for industrial micromachining. PERLA platform provides sub-1-ps laser pulses with excellent power stability and beam quality as low as 1.1 at 1030 nm and its harmonic frequencies. Such laser are an excellent tool, especially for multi-beam micromachining. Ability of PERLA platform in this field was demonstrated on direct laser interference patterning of steel, invar, and tungsten with perfect results.

Funding. Technology Agency of the Czech Republic (TN01000008); Horizon 2020 Framework Programme (739573); European Regional Development Fund (CZ.02.1.01/0.0/0.0/15_006/0000674).

Disclosures. The authors declare no conflicts of interests

References

1. J. Bonse, S. V. Kirner, S. Höhm, N. Epperlein, D. Spaltmann, A. Rosenfeld, and J. Krüger, "Applications of laser-induced periodic surface structures (LIPSS)," *Proc. SPIE 10092, Laser-based Micro- and Nanoprocessing XI*, 100920N (17 February 2017)
2. X. Liu, D. Du, and G. Mourou, "Laser ablation and micromachining with ultrashort laser pulses," IEEE J. Quantum Electron. **33**(10), 1706–1716 (1997).
3. A. Y. Vorobyev and C. Guo, "Direct femtosecond laser surface nano/microstructuring and its applications," Laser Photonics Rev. **7**(3), 385–407 (2013).
4. J. Bonse, J. Krüger, S. Höhm, and A. Rosenfeld, "Femtosecond laser-induced periodic surface structures," J. Laser Appl. **24**(4), 042006 (2012).
5. G. Lazzini, L. Gemini, A. Lutey, R. Kling, L. Romoli, M. Allegrini, and F. Fuso, "Surface Morphologies in Ultra-short Pulsed Laser Processing of Stainless-Steel at High Repetition Rate," Int. J. Precis. Eng. Manuf. **20**(9), 1465–1474 (2019).
6. A. Lasagni, A. Manzoni, and F. Mücklich, "Micro/Nano Fabrication of Periodic Hierarchical Structures by Multi-Pulsed Laser Interference Structuring," Adv. Eng. Mater. **9**(10), 872–875 (2007).
7. P. Hauschwitz, D. Jochcová, R. Jagdheesh, D. Rostohar, J. Brajer, J. Kopeček, M. Cimrman, M. Smrž, T. Mocek, and A. Lucianetti, "Towards rapid large-scale LIPSS fabrication by 4-beam ps DLIP," Opt. Laser Technol. **133**, 106532 (2021).
8. P. Hauschwitz, D. Jochcová, R. Jagdheesh, M. Cimrman, J. Brajer, D. Rostohar, T. Mocek, J. Kopeček, A. Lucianetti, and M. Smrž, "Large-Beam Picosecond Interference Patterning of Metallic Substrates," Materials **13**(20), 4676 (2020).
9. M. Smrž, O. Novák, J. Mužík, H. Turčičová, M. Chyla, S. S. Nagisetty, M. Vyvlečka, L. Roškot, T. Miura, J. Černohorská, P. Sikocinski, L. Chen, J. Huynh, P. Severová, A. Pranovich, A. Endo, and T. Mocek, "Advances in High-Power, Ultrashort Pulse DPSSL Technologies at HiLASE," Appl. Sci. **7**(10), 1016 (2017).
10. A. Giesen, H. Hügel, A. Voss, K. Wittig, U. Brauch, and H. Opower, "Scalable concept for diode-pumped high-power solid-state lasers," Appl. Phys. B **58**(5), 365–372 (1994).

OSA CONTINUUM

11. S. S. Schad, C. Stolzenburg, K. Michel, and D. Sutter, "Latest Advances in High Brightness Disk Lasers," Laser Tech. J. **11**(2), 49–53 (2014).
12. J.-P. Negel, A. Loescher, A. Voss, D. Bauer, D. Sutter, A. Killi, M. A. Ahmed, and T. Graf, "Ultrafast thin-disk multipass laser amplifier delivering 1.4 kW (4.7 mJ, 1030 nm) average power converted to 820 W at 515 nm and 234 W at 343 nm," Opt. Express **23**(16), 21064–21077 (2015).
13. T. Nubbemeyer, M. Kaumanns, M. Ueffing, M. Gorjan, A. Alismail, H. Fattahi, J. Brons, O. Pronin, H. G. Barros, Z. Major, T. Metzger, D. Sutter, and F. Krausz, "1 kW, 200 mJ picosecond thin-disk laser system," Opt. Lett. **42**(7), 1381–1384 (2017).
14. R. Jung, J. Tümmler, T. Nubbemeyer, and I. Will, "Thin-disk ring amplifier for high pulse energy," Opt. Express **24**(5), 4375–4381 (2016).
15. C. Herkommer, P. Krötz, R. Jung, S. Klingebiel, C. Wandt, R. Bessing, P. Walch, T. Produit, K. Michel, D. Bauer, R. Kienberger, and T. Metzger, "Ultrafast thin-disk multipass amplifier with 720 mJ operating at kilohertz repetition rate for applications in atmospheric research," Opt. Express **28**(20), 30164–30173 (2020).
16. S. Erhard, A. Giesen, M. Karszewski, T. Rupp, C. Stewen, I. Johannsen, and K. Contag, "Novel Pump Design of Yb:YAG Thin Disc Laser for Operation at Room Temperature with Improved Efficiency," *Advanced Solid State Lasers*, M. Fejer, H. Injeyan, and U. Keller, eds., Vol. 26 of OSA Trends in Optics and Photonics (Optical Society of America, 1999), paper MC3.
17. K. Contag, M. Karszewski, C. Stewen, A. Giesen, and H. Hugel, "Theoretical modelling and experimental investigations of the diode-pumped thin disk Yb:YAG laser," Quantum Electron. **29**(8), 697–703 (1999).
18. K. Schuhmann, T. W. Hänsch, K. Kirch, A. Knecht, F. Kottmann, F. Nez, R. Pohl, D. Taqqu, and A. Antognini, "Thin-disk laser pump schemes for large number of passes and moderate pump source quality," Appl. Opt. **54**(32), 9400–9408 (2015).
19. J. Preclíková, K. Bartoš, J. Kubát, M. Košelja, B. Rus, M. Divoký, T. Mocek, and J. Houžvička, "Large Scale Single Crystal Growth," in *Laser Congress 2018 (ASSL), OSA Technical Digest* (Optical Society of America, 2018), paper AM4A.1.
20. M. Divoky, J. Pilar, M. Hanus, P. Navratil, M. Sawicka-Chyla, M. De Vido, P. J. Phillips, K. Ertel, T. Butcher, M. Fibrich, J. T. Green, M. Koselja, J. Preclikova, J. Kubat, J. Houzvicka, B. Rus, J. Collier, A. Lucianetti, and T. Mocek, "Performance comparison of Yb:YAG ceramics and crystal gain material in a large-area, high-energy, high average–power diode-pumped laser," Opt. Express **28**(3), 3636–3646 (2020).
21. J. Körner, J. Hein, M. Kahle, H. Liebetrau, M. Lenski, M. Kaluza, M. Loeser, and M. Siebold, "Temperature dependent measurement of absorption and emission cross sections for various Yb3+ doped laser materials," *Proceedings of SPIE Optics + Optoelectronics conference, Prague, Czech Republic*, Jun 2011 (Proceedings SPIE 8080, 2011), pp. 8080
22. B. Weichelt, A. Voss, M. A. Ahmed, and T. Graf, "Enhanced performance of thin-disk lasers by pumping into the zero-phonon line," Opt. Lett. **37**(15), 3045–3047 (2012).
23. M. Smrž, T. Miura, M. Chyla, S. S. Nagisetty, O. Novák, A. Endo, and T. Mocek, "Suppression of nonlinear phonon relaxation in Yb:YAG thin disk via zero phonon line pumping," Opt. Lett. **39**(16), 4919–4922 (2014).
24. P. Severová, S. S. Nagisetty, T. Miura, A. Endo, M. Smrž, and T. Mocek, "Investigation of spectrally-dependent phonon relaxation mechanism in Yb:YAG gain media and its consequences for thin disk laser performance," Laser Phys. **30**(2), 025005 (2020).
25. T. Miura, M. Chyla, M. Smrž, S. S. Nagisetty, P. Severová, O. Novák, A. Endo, and T. Mocek, "In-situ optical phase distortion measurement of Yb:YAG thin disk in high average power regenerative amplifier," *Proc. SPIE 8603, High-Power Laser Materials Processing: Lasers, Beam Delivery, Diagnostics, and Applications II*, 860303 (26 February 2013).
26. K. Schuhmann, K. Kirch, F. Nez, R. Pohl, and A. Antognini, "Thin-disk laser scaling limit due to thermal lens induced misalignment instability," Appl. Opt. **55**(32), 9022–9032 (2016).
27. S. S. Nagisetty, P. Severova, T. Miura, M. Smrž, H. Kon, M. Uomoto, T. Shimatsu, M. Kawasaki, T. Higashiguchi, A. Endo, and T. Mocek, "Lasing and thermal characteristics of Yb:YAG/YAG composite with atomic diffusion bonding," Laser Phys. Lett. **14**(1), 015001 (2017).
28. D. Strickland and G. Mourou, "Compression of amplified chirped optical pulses," Opt. Commun. **56**(3), 219–221 (1985).
29. W. H. Renninger, A. Chong, and F. W. Wise, "Pulse Shaping and Evolution in Normal-Dispersion Mode-Locked Fiber Lasers," IEEE J. Sel. Top. Quantum Electron. **18**(1), 389–398 (2012).
30. O. Novák, T. Miura, M. Smrž, M. Chyla, S. S. Nagisetty, J. Mužík, J. Linnemann, H. Turčičová, V. Jambunathan, O. Slezák, M. Sawicka-Chyla, J. Pilař, S. Bonora, M. Divoký, J. Měsíček, A. Pranovich, P. Sikocinski, J. Huynh, P. Severová, P. Navrátil, D. Vojna, L. Horáčková, K. Mann, A. Lucianetti, A. Endo, D. Rostohar, and T. Mocek, "Status of the High Average Power Diode-Pumped Solid State Laser Development at HiLASE," Appl. Sci. **5**(4), 637–665 (2015).
31. P. Peterka, P. Koška, and J. Čtyroký, "Reflectivity of superimposed Bragg gratings induced by longitudinal mode instabilities in fiber lasers," IEEE J. Sel. Top. Quantum Electron. **24**(3), 1–8 (2018).
32. J. Dörring, A. Killi, U. Morgner, A. Lang, M. Lederer, and D. Kopf, "Period doubling and deterministic chaos in continuously pumped regenerative amplifiers," Opt. Express **12**(8), 1759–1768 (2004).

OSA CONTINUUM

33. M. Smrž, M. Chyla, O. Novák, T. Miura, A. Endo, and T. Mocek, "Amplification of picosecond pulses to 100 W by an Yb:YAG thin-disk with CVBG compressor," *Proc. SPIE 9513, High-Power, High-Energy, and High-Intensity Laser Technology II*, 951304 (12 May 2015).
34. L. B. Glebov, "Volume holographic elements in a photo-thermo-refractive glass," J. Holography Speckle **5**(1), 77–84 (2009).
35. L. B. Glebov, V. Smirnov, E. Rotari, I. Cohanoschi, L. Glebova, O. Smolski, J. Lumeau, C. Lantigua, and A. Glebov, "Volume-chirped Bragg gratings: monolithic components for stretching and compression of ultrashort laser pulses," Opt. Eng. **53**(5), 051514 (2014).
36. D. Štěpánková, J. Mužík, O. Novák, L. Roškot, V. Smirnov, L. Glebov, M. Jelínek, M. Smrž, A. Lucianetti, and T. Mocek, "Experimental study on compression of 216-W laser pulses below 2 ps at 1030 nm with chirped volume Bragg grating," Appl. Opt. **59**(26), 7938–7944 (2020).
37. S. Cho, O. Novák, M. Smrž, A. Lucianetti, T. J. Yu, and T. Mocek, "Numerical analysis of beam distortion induced by thermal effects in chirped volume Bragg grating compressors for high-power lasers," J. Opt. Soc. Am. B **37**(12), 3874–3881 (2020).
38. E. Treacy, "Optical pulse compression with diffraction gratings," IEEE J. Quantum Electron. **5**(9), 454–458 (1969).
39. H. Turcicova, O. Novak, L. Roskot, M. Smrz, J. Muzik, M. Chyla, A. Endo, and T. Mocek, "New observations on DUV radiation at 257 nm and 206 nm produced by a picosecond diode pumped thin-disk laser," Opt. Express **27**(17), 24286–24299 (2019).
40. O. Novák, H. Turčičová, M. Smrž, T. Miura, A. Endo, and T. Mocek, "Picosecond green and deep ultraviolet pulses generated by a high-power 100 kHz thin-disk laser," Opt. Lett. **41**(22), 5210–5213 (2016).
41. P. Hauschwitz, B. Stoklasa, J. Kucharik, H. Turcicova, M. Pisarik, J. Brajer, D. Rostohar, T. Mocek, M. Duda, and A. Lucianetti, "Micromachining of Invar with 784 Beams Using 1.3 ps Laser Source at 515 nm," Materials **13**(13), 2962 (2020).
42. H. Sopha, I. Mirza, H. Turčičová, D. Pavlinak, J. Michalicka, M. Krbal, J. Rodriguez-Pereira, L. Hromadko, O. Novák, J. Mužík, M. Smrž, E. Kolíbalová, N. Goodfriend, N. M. Bulgakova, T. Mocek, and J. Macák, "Laser-induced crystallization of anodic TiO2 nanotube layers," RSC Adv. **10**(37), 22137–22145 (2020).
43. M. Smrž, M. Chyla, J. Mužík, S. S. Nagisetty, and O. Novák, "Compact, picosecond, kW-class laser thin-disk laser PERLA for hi-tech industrial applications," MM Science Journal **2019**, 3620–3625 (2019).